# Flower morphology as a predictor of pollination mode in a biotic to abiotic pollination continuum

Jesús Martínez-Gómez<sup>1,2†</sup>, Seongjun Park<sup>3†</sup>, Samantha R. Hartogs<sup>1</sup>, Valerie L. Soza<sup>1</sup>, SeonJoo Park<sup>4</sup>
and Verónica S. Di Stilio<sup>1\*</sup>

<sup>1</sup>Department of Biology, University of Washington, PO BOX 351800, Seattle, WA
98195, USA; <sup>2</sup>School of Integrative Plant Sciences and L.H. Bailey Hortorium, Cornell
University, Ithaca, New York 14853, USA; <sup>3</sup>Institute of Natural Science, Yeungnam
University, Gyeongsan, Gyeongbuk, 38541, South Korea; <sup>4</sup>Department of Life
Sciences, Yeungnam University, Gyeongsan, Gyeongbuk, 38541, South Korea
\*For correspondence. E-mail distilio@uw.edu

<sup>†</sup>Equal contribution

- Background and Aims Wind pollination has evolved repeatedly in flowering plants, yet the identification of a wind pollination syndrome as a set of integrated floral traits can be elusive. *Thalictrum* (Ranunculaceae) comprises temperate perennial herbs that have transitioned repeatedly from insect to wind pollination while also exhibiting mixed pollination, providing an ideal system to test for evolutionary correlation between floral morphology and pollination mode in a biotic to abiotic continuum. Moreover, the lack of floral organ fusion across this genus additionally allows to test for specialization to pollination vectors in the absence of this feature.
- Methods We expanded phylogenetic sampling in the genus from a previous study using six chloroplast loci, which allowed us to test whether species cluster into distinct pollination syndromes based on floral morphology. We then used multivariate analyses on floral traits, followed by ancestral state reconstruction of the emerging flower morphotypes and determined whether these traits are evolutionarily correlated under a Bayesian framework with Brownian motion.
- **Key Results** Floral traits fell into five distinct clusters, which were reduced to three after considering phylogenetic relatedness, and were largely consistent with flower morphotypes and associated pollination vectors. Multivariate evolutionary analyses found a positive correlation between the lengths of floral reproductive structures (styles, stigmas, filaments, and anthers). Shorter reproductive structures tracked insect-pollinated species and clades in the phylogeny while longer structures tracked wind-pollinated ones, consistent with selective pressures exerted by biotic vs. abiotic pollination vectors, respectively.
- **Conclusions** While detectable suites of integrated floral traits across *Thalictrum* correlated with wind or insect pollination at the extremes of the morphospace

distribution, a presumed intermediate, mixed pollination mode morphospace was also detected. Thus, our data broadly support the existence of detectable flower morphotypes from convergent evolution underlying pollination mode evolution in *Thalictrum*, presumably via different paths from an ancestral mixed pollination state.

**Key words:** ambophily, anemophily, entomophily, evolutionary correlation, flower morphology, integration, multivariate Brownian motion, phylogenetic comparative methods, pollination syndrome, pollination mode, *Thalictrum* (Ranunculaceae), wind pollination.

## INTRODUCTION

Pollination mode, a key life-history feature of seed plants, refers to the process by which pollen is transferred between male (anthers) and female (stigma) reproductive structures, which can occur by proximity (selfing) or via biotic or abiotic agents. Multiple aspects of floral diversity are shaped by selective pressures exerted by pollinating agents, e.g., flower shape (Smith and Kriebel 2018), flower size and floral display (Parachnowitsch and Kessler 2010), and nectar spur length (Whittall and Hodges 2007). Convergent evolution on the same type of pollinator may result in analogous suites of floral morphologies, or a pollination syndrome (Fenster *et al.* 2004). Theoretical as well as empirical evidence suggests that pollinator selection may act on multiple organs within a flower (Stebbins 1951; Fenster *et al.* 2015). Alternatively, selection on one floral organ may impact others due to developmental correlation (e.g., genetic linkage, pleiotropy, or structural constraint, Smith 2016). Either of these scenarios results in evolutionary integration, where structures evolve in a correlated fashion within a flower under the selection pressure exerted by pollinators (Berg 1960).

A special case of evolutionary integration within flowering plants is synorganization, where floral organs function as a morphological unit due to whorled phyllotaxis and fusion, most commonly syncarpy and sympetaly (Endress 2016). For example, petals are fused into a corolla tube (sympetaly) in many flowering plants, with variation in corolla tube size and shape emerging from specialized pollination modes. To date, evolutionary correlation between flower organs (as a proxy for integration) has only been studied in such flowers, with synorganization arising from organ fusion (Lagomarsino *et al.* 2017; Joly *et al.* 2018; Smith and Kriebel 2018; Dellinger *et al.* 2019; Kriebel *et al.* 2020).

Here, we test whether evolutionary integration of floral organs can occur in the absence of whorled phyllotaxis and organ fusion in a non-core eudicot lineage with a variable floral ground plan (Kitazawa and Fujimoto 2014; Kitazawa 2021). *Thalictrum* (Ranunculaceae) consists of approximately

200 species that display variation in pollination mode, sexual system, and ploidy level (Tamura 1995). The genus lacks any form of floral organ fusion or whorled phyllotaxy—where organ primordia of the same kind develop synchronously—arising instead in a spiral or irregular whorl.

Despite this absence of preconditions for synorganization (Endress 2016; Phillips *et al.* 2020) in its floral ground plan, distinct suites of floral characters associated with different pollinating agents can be identified in *Thalictrum*: generalist insect pollination (entomophily); more specialized wind pollination (anemophily) that evolved at least eight times (Wang *et al.* 2019); and pollination by both insects and wind (ambophily), hypothesized as either an evolutionary intermediate step or a stable state (Culley *et al.* 2002).

Charles Darwin (1862) famously drew on evidence of extremely long nectar spurs in the Madagascan orchid Angraecum sesquipedale to correctly predict a hawkmoth pollinator with an equally long proboscis. Yet, the predictive value of floral morphology varies widely and may be casespecific, and the applicability of this concept across angiosperms is contentious at best (Ollerton et al. 2009, 2015; Rosas-Guerrero et al. 2014). Establishing a species' pollination mode is a timeconsuming task that requires studying plants in their natural environment, and while this remains the golden standard, statistical methods can help identify predictive morphologies by generating a training dataset from a subsample of species with known pollination mode (Lagomarsino et al. 2017; Dellinger et al. 2019; van der Niet 2021). Such an approach could facilitate, in turn, macroevolutionary analyses requiring large datasets to further investigate the mechanisms underlying the evolution of different modes of pollination. Ecological studies of pollination mode in natural populations have been conducted for 13 Thalictrum species (Kaplan and Mulcahy 1971; Melampy and Hayworth 1980; Davis 1997; Steven and Waller 2004; Guzmán 2005; Humphrey 2018). A 'pollination index' (PI) was previously devised to predict pollination mode from morphology in the absence of field data (Kaplan and Mulcahy 1971). This pollination index involves qualitatively scoring and then averaging seven floral characters considered indicative of pollination syndrome: flower color, flower size, anther and stigma length, filament orientation, and stamen and pistil exsertion. A

PI value of 1 is assigned to anemophily, 3 to entomophily, and 2 to ambophily (Kaplan and Mulcahy 1971). Here, we build upon and refine this pollination index using quantitative traits and phylogenetic comparative methods to further increase the predictive value of flower morphology in assessing pollination mode.

In this study, we aimed to 1) investigate the predictive power of continuous floral traits in distinguishing pollination mode within an improved phylogenetic context in *Thalictrum* (Ranunculaceae), 2) reconstruct the evolution of flower morphotypes in the genus, and 3) assess the degree of evolutionary correlation (integration) between floral traits in a phylogenetic context. To that end, we first inferred a chronogram with increased taxon and molecular sampling that constituted the framework of our phylogenetic comparative methods. We then tested the predictive value of floral morphology in assigning pollination mode by Principal Component Analysis (PCA) and K-means clustering and reconstructed the evolution of the resulting flower morphotypes. Lastly, to identify suites of correlated floral traits that may be contributing to pollination syndromes, we characterized the degree of evolutionary integration between floral organs using multivariate Brownian motion models in a Bayesian framework.

# **METHODS**

Taxon sampling

Ninety-nine taxa were sampled (Appendix 1), comprising 93 recognized species that spanned all 14 currently recognized sections of *Thalictrum* (Tamura 1995) and the group's geographic distribution and morphological diversity. *Aquilegia buergeriana* var. *oxysepala*, *A. formosa*, *Enemion raddeanum*, *Isopyrum manshuricum*, *Leptopyrum fumarioides*, *Semiaquilegia adoxoides*, and *Paraquilegia microphylla* were chosen as outgroups based on previous studies (Park *et al.* 2015; Wang *et al.* 2019).

DNA extraction, amplification, and sequencing

Total genomic DNA was isolated from fresh leaves or herbarium specimens as described in Park et al. (2015) and Soza et al. (2012). Six plastid regions (ndhA intron, ndhF, rbcL, trnL intron, trnL-F intergenic spacer [IGS], and rpl32-trnL IGS) were amplified using primers in Shaw et al. (2007) or designed for this study [Supplementary data Table S1]. Polymerase chain reaction (PCR) was performed in 30  $\mu$ L, including DiaStar-Taq DNA polymerase (SolGent Co., Daejeon, Korea) or GoTaq Master Mix (Promega, Madison, WI) and 1  $\mu$ L of genomic DNA (2-50 ng). Cycling conditions were 95°C for 2-3 min; 30-40 cycles of 95°Gor 30-60 sec, 46-60°Gor 40-60 sec, and 72°Gor 50-150 sec; and 72°C for 5 min. Sequencing of PCR products was performed at SolGent Co. or Genewiz (Seattle, USA).

# Phylogenetic analyses

For each plastid region, raw sequences were assembled into contigs, and consensus sequences were aligned with MUSCLE (Edgar 2004) in Geneious R7. Phylogenetic reconstructions were performed on a concatenated alignment of six plastid regions. Maximum likelihood (ML) analyses were performed using IQ-TREE v1.6.8 (Nguyen *et al.* 2015) under best-fitting partition schemes from ModelFinder (Kalyaanamoorthy *et al.* 2017) [Supplementary data Table S2]. Branch support came from 1,000 ultrafast bootstrap (bs) replicates. Bayesian inference (BI) was conducted using MrBayes v.3.2 (Ronquist *et al.* 2012) with two runs of Markov Chain Monte Carlo (MCMC) for 12,000,000 generations each and trees sampled every 100 generations. The model of molecular evolution was selected with the corrected Akaike information criterion (AICc) (Hurvich and Tsai 1989) using jModelTest v.2.1.10 (Posada 2008). MCMC convergence was assessed from the effective sampling size (ESS) of the combined runs. All parameter estimates had ESS >1,000 after burn-in (first 25% of generations discarded), indicating that the analyses had sampled the posterior distributions

satisfactorily. Posterior probability (PP) of branches was estimated from the 50% majority-rule consensus tree.

## Divergence time estimation

Divergence times and topology were jointly estimated using a Bayesian MCMC method in BEAST v.2.5.2 (Drummond *et al.* 2012). The dataset was partitioned by each chloroplast region and its optimal model. We used a relaxed clock model (Drummond *et al.* 2006) and a Yule process of speciation as a tree prior. A secondary calibration point, based on a published divergence time estimate for the genus *Thalictrum* from a densely sampled Ranunculaceae chronogram (Fior *et al.* 2013), was used for the root age constraint with a normal prior distribution (mean = 26.2, SD = 3.6, and range = 20.3-32.3 million years ago [mya]). Analyses were run for 100,000,000 generations, sampling every 1,000 generations. The posterior distribution of all parameters was examined in Tracer v.1.7 (Rambaut *et al.* 2018). ESS was greater than 1,000 after 10% of samples were discarded as burn-in. A maximum clade credibility (MCC) chronogram was generated with TreeAnnotator v.1.7.1 (Drummond *et al.* 2012) showing mean divergence time estimates with 95% highest posterior density (HPD) intervals.

# Flower morphology

We measured 17 floral characters from 29 species (including 10 out of 13 taxa with empirical pollination mode data) from flatbed scans (Epson Perfection V39) of fresh flowers [Supplementary data Fig. S1]. Plants were grown in the University of Washington Greenhouse from wild-collected seed or purchased as adult plants from nurseries [Supplementary data Table S3]. Flowers were scanned after dissecting their sepals, when anthers were beginning to dehisce in the outer stamens and before fertilization. A 100 cm x 50 cm area was scanned at 1200-2400 dpi with a ruler for scale.

ImageJ's (Schneider *et al.* 2012) straight line or segmented line tool was used to measure three each of the following traits per flower (in mm): sepal length, sepal width, filament length, maximum filament width, minimum filament width, anther length (including mucron when present, an extension of sterile tissue at the anther apex), anther width, stigma length, stigma width at base, stigma width at apex, style length, style width at base, ovary length, ovary width, and gynophore length (when present, a stalk that elevates the gynoecium). To account for intraspecific variation, at least three organs of each type (sepals, stamens, and carpels) per flower and three flowers from two to three plants per species and per sex (for dioecious and monoecious species) were measured. Missing organs were assigned a value of zero. *Thalictrum revolutum* female flowers and *T. pubescens* were measured from herbarium specimens and fixed specimens, respectively.

## Pollination index

Pollination index data were compiled from the literature (Kaplan and Mulcahy 1971; Soza *et al.* 2012, 2013; Wang *et al.* 2019) or newly calculated from images (Global Biodiversity Information Facility) for a total of 83 species.

# Multivariate analysis of floral traits

Trait averages per flower (excluding count data) were log-transformed, adding 1 to zeros. Analyses were performed with base R functions (R Core Team 2018), unless specified otherwise. PCA was performed on raw, replicate continuous trait values (without species averages) and on the pollination index dataset (on species averages). K-means clustering analysis was performed with 10,000 iterations, and the optimal k was determined with NbClust (Charrad *et al.* 2014) using majority-rule criteria from 30 goodness-of-fit metrics. Screen plot identified the number of PCs including at least 80% of the total variance (Jolliffe 2002). Ten species with validated pollination

mode were used to assign the type of pollination within their K-means cluster (Table 1). Sexual dimorphism in sepal size was tested with one-way ANOVA.

Phylogenetic comparative methods

Phylogenetic PCA: The estimated chronogram from above was trimmed to the 29 taxa with floral trait data using phytools (Revell 2012). All species were monophyletic on the trimmed phylogeny except *T. aquilegiifolium*; we chose accession Kawahara & al. 666 [TI] to represent this species. Phylogenetic PCA was performed under a model of Brownian motion and lambda with the phyl.pca function (Revell 2009) in phytools (Revell 2012).

Ancestral state reconstruction of flower morphology Ancestral flower morphotype was inferred by fitting a continuous-time Markov model of discrete character evolution in corHMM (Boyko and Beaulieu 2021). 'Equal rates,' 'symmetrical rates,' and 'all rates different' models under 'equal', 'empirical' and 'stationary' root priors (nine models total), were fitted using the rayDISC function.

The AICc was used to select the best-fitting model. To estimate the number of transitions between character states, we implemented stochastic character mapping with make.simmap in phtyools to simulate 1000 character histories under the best fit model (Revell 2012). Two cases where different flowers from the same species did not fall within the same cluster (*T. delavayi* and *T. petaloideum*) were scored based on the cluster with majority representation.

Evolutionary correlation of floral traits We aimed to identify statistical correlations among floral traits, accounting for within-species variation and phylogenetic relationships while accommodating missing data due to sexual system variation. To that end, we inferred the evolutionary rate matrix under a model of multivariate Brownian motion (Revell and Harmon 2008). This matrix describes both the rates of evolution of individual traits and the evolutionary covariance (correlation coefficient) between pairs of traits, allowing us to test whether pairs of traits are evolutionary correlated or independent of each other. We fit a multivariate Brownian motion model of correlated evolution for all pairwise combinations of traits using the R package MCMCglmm (Hadfield 2010),

with parameter-expanded uninformative priors. In addition to direct measurements, we included three composite traits: stamen length (filament length + anther length), carpel length (ovary length + style length), and anther size (anther length x anther width). Given that stigmatic papillae mostly run along the style in *Thalictrum* and the two measurements often coincide, we chose to use style length (together with ovary length) for the carpel length estimate. Gaussian distributions (Brownian motion) and Poisson distributions were used to model the evolution of continuous traits and flower organ counts, respectively. Three MCMC chains were run for 100,000 iterations until convergence (ESS>200 for all parameters), as calculated by CODA (Plummer *et al.* 2006). Correlation coefficients that did not overlap with zero were considered significant (Harmon 2018). The 95% confidence interval for posterior distributions was calculated with LaplacesDemon (Statisticat 2021). Maximum a posteriori (MAP) estimates from RevGadgets were used to summarize posterior distributions (Tribble *et al.* 2022). Plots were generated with ggplot2, Cowplot, and ggtree (Wickham 2011; Yu *et al.* 2017; Wilke 2020).

We tested whether floral traits showed evolutionary correlation for all pairwise combinations (except gynophore length, present in 9/29 species and hence not amenable to this type of analysis). Dioecious taxa have sepal data from staminate and carpellate flowers, while andromonoecious taxa (staminate and hermaphroditic flowers on the same plant) and cryptically dioecious *T. pubescens* (male-sterile hermaphroditic flowers and staminate flowers on separate plants) have sepal and stamen data from staminate and hermaphroditic flowers. To account for this intraspecific flower dimorphism, two types of analyses were performed: on reproductive organs (stamens and carpels) and on all organs (including sepals). For reproductive organs, we combined stamen and carpel measurements from different flowers (dioecious taxa) or averaged stamen measurements between male and hermaphroditic flowers (andromonoecious taxa). This enabled the computation of phylogenetic correlations between stamen and carpel traits found on separate flowers within a species. For all floral organs (perianth included), we divided the data into a "carpellate dataset" (carpellate + hermaphroditic flowers) and a "staminate dataset" (staminate +

hermaphroditic flowers), with stamen and sepal averages across flower types for andromonoecious species. This analysis allowed us to infer evolutionary correlations between the perianth and reproductive organs, while also accounting for sexual dimorphism of sepals.

## RESULTS

An expanded phylogeny for Thalictrum

The current phylogeny has the most comprehensive sampling to date for the genus, 93 out of 196 species (47% taxon coverage), using six concatenated chloroplast regions to improve resolution and support along the backbone, with all but one node strongly supported (i.e., bs > 75% and PP  $\ge 0.95$ ) [Supplementary data Figs. S2, S3]. Consistent with prior analyses (Soza *et al.* 2012, 2013; Wang *et al.* 2019), the current phylogeny identified two major clades (I and II) in the genus and three strongly supported subclades in clade II with divergent sexual systems: one consisting mostly of andromonoecious species (except for hermaphroditic *T. decipiens*, renamed as subclade A) and two consisting of dioecious species (renamed as subclades B and C).

The plastid dataset was subsequently used to reconstruct a chronogram with Bayesian divergence estimation and one calibration point (Fig. 1), which was implemented in subsequent analyses. Resulting divergence estimates that coincided with previously supported clades were within range of previous estimates (Soza *et al.* 2013): a crown age of 8.9-21.8 mya for *Thalictrum*, 4.8-13.4 mya for clade I, 6.6-16.9 mya for clade II, 1.6-5.3 mya for clade A, 0.9-2.7 mya for clade B, and 0.9-3.4 mya for clade C.

Distinct flower morphotypes associate with different pollination modes

To address whether suites of integrated floral traits segregate species by pollination mode, we sampled continuous floral traits across the genus, representing all major clades and floral

morphotypes. *Thalictrum* flowers exhibited a wide range of variation in flower morphology that included a more than threefold difference in the sum of all trait values, a potential proxy for floral size [Supplementary data Fig. S4A]. Within-species variation was also present in dioecious and andromonoecious taxa as sexual dimorphism of sepals, which were larger (longer and/or wider) in staminate flowers compared to carpellate or hermaphroditic flowers [Supplementary data Fig. S4B], a relationship previously reported for other unisexual wind-pollinated species, including *T. dioicum* (Delph *et al.* 1996).

The first four principal components (PCs) in multivariate analyses explained the majority of the total variance (83.23% combined) [Supplementary data Fig. S5A], resulting in five K-means clusters [Supplementary data Fig. S5B] best visualized in PC1 vs. PC3 (Fig. 2a) [Supplementary data Fig. S5C-D]. PC1 segregated the data into distinct carpellate (green, left), hermaphroditic (gray+blue+pink, center), and staminate (yellow, right) clusters (Fig. 2a) [Supplementary data Video **S1]**, with predominant contributions from carpel and stamen traits (left- and right-pointing biplot vectors, respectively, Fig. 2b) and was therefore interpreted as a sexual system axis. PC2 segregated flowers that had a higher sum of all trait values from those with a lower sum of all trait values, a potential proxy for flower size [Supplementary data Fig. S5C, E, biplot vectors pointing down]. PC3 further separated the three hermaphroditic clusters, distinguishing flowers with larger petaloid sepals and narrower (filiform to weakly dilated, i.e. wider at the top) stamen filaments (e.g., T. thalictroides, Fig. 2a pink cluster) from those with smaller, early deciduous sepals and wider (strongly dilated or clavate) stamen filaments, resulting in showier stamens, and carpels elevated on gynophores (e.g., T. aquilegiifolium; Fig. 2a gray cluster and Fig. 2b, biplot vectors for sepal width and length, filament width, and gynophore length). Finally, PC4 separated species with shorter reproductive organs and more sepals, such as T. thalictroides, from those with longer reproductive organs and fewer sepals like T. hernandezii [Supplementary data Fig. S5D, F, biplot vector for style, stigma, anther, and filament length]. In summary, hermaphroditic flowers fell into three morphotypes: "petaloid sepals," "showy stamens," and "intermediate" with small white sepals,

white filiform or weakly dilated stamen filaments, and yellow anthers (e.g., *T. lucidum*, Fig. 2a blue cluster). We called this morph "intermediate" because, while none of these flowers have large petaloid sepals nor strongly dilated filaments, their white and weakly dilated filaments and nongreen sepals make them potentially attractive to insects. Hermaphroditic flowers of sexually dimorphic taxa, including cryptically dioecious *T. pubescens* (Kaplan and Mulcahy 1971; Davis 1997) and andromonoecious *T. hernandezii* and *T. guatemalense*, were found at the boundary of the intermediate cluster (Fig. 2a, circled blue symbols). Likewise, staminate flowers of *T. pubescens* were found on the edge of the staminate cluster (Fig. 2a, circled yellow symbols).

To prevent circularity in assigning pollination mode from morphology based on K means, we validated pollination mode for each cluster based on membership by species whose pollination mode had been investigated in the field (Table 1, Fig. 2a filled symbols). The petaloid sepal cluster was designated as insect-pollinated based on *T. thalictroides* membership while the showy stamen cluster was designated as insect-pollinated based on *T. clavatum* and *T. aquilegiifolium*. Staminate and carpellate clusters were classified as wind-pollinated based on *T. fendleri, T. dioicum,* and *T. revolutum*. The intermediate cluster was unresolved with respect to pollination mode, containing ambophilous *T. pubescens* (hermaphroditic flowers), wind-pollinated *T. alpinum* and *T. minus*, and insect-pollinated *T. flavum*. In summary, while the edges of the PCA could be more readily assigned to insect or wind pollination, complexity in the data resulted in representatives of each of the three potential syndromes (wind, insect, or ambophily) at the center of the morphospace, representing an intermediate flower morphotype unresolved with respect to pollination mode.

The integration of phylogenetic relationships via phylogenetic PCA (pPCA) and species averages reduced the number of distinct morphological clusters from five to three (Fig. 2c, K = 3, color-coding as in Fig. 2d), underscoring the importance of shared evolutionary history and species-level variation. pPC1 explained the majority of the variance (94.91%), largely discriminating taxa with petaloid sepals validated as insect-pollinated at the far left (e.g., *T. thalictroides*, pink) from

unisexual flowers validated as wind-pollinated at the far right (e.g., *T. dioicum*, citrine). This pattern along pPC1 largely matches the distribution of species along PC2 (Fig 2c bottom inset)

[Supplementary data Fig. S5C], suggesting that the associated floral trait combinations are mostly independent of shared ancestry (i.e., certain trait clusters remain distinct despite being weighted by the phylogenetic variance-covariance matrix), and hence convergent evolution to pollination vector is one likely explanation. Exceptions to that match include a member of the petaloid sepal group, *T. delavayi*, that fell into the middle cluster in pPCA (Fig. 2c), suggesting less distinction (less data granularity) when using species averages and phylogeny. Flowers with showy stamens and intermediate flower morphotypes were distributed across all three pPCA clusters, implying that the trait contribution to those morphotypes was decreased when accounting for phylogeny. For the showy stamen cluster, gynophore length and the maximum width of the stamen filaments were the largest discriminating trait contributions (Fig. 2b, upward arrows) that were presumably attenuated in the pPCA. Taken together, phylogenetically informed multivariate analysis in *Thalictrum* still broadly discriminated between insect-pollinated flower types with petaloid sepals and wind-pollinated small and mostly unisexual flower types.

An intermediate, transitional flower type is inferred as the ancestral state for clade II

Since the intermediate cluster from PCA contains taxa with all three pollination modes that are morphologically intermediate between those in the wind and insect clusters (Fig. 2a), we asked whether it represents the ancestral condition for clade II (Fig. 1), where all major transitions occurred (to polyploidy, wind pollination, and unisexual flowers, Soza *et al.* 2012, 2013). To test this hypothesis, we inferred discrete ancestral states using the K-means cluster scheme on a trimmed phylogeny of the 29 species with flower trait data, representing all major clades (Fig. 2d). To properly capture all flower morphotypes emerging from the K-means analysis, sexually dimorphic species were assigned the combined score [staminate+intermediate] for andromonoecy (*T. guatemalense* and *T. hernandezii*) and cryptic dioecy (staminate and male-sterile hermaphroditic

flowers, T. pubescens) or [staminate + carpellate] for dioecious species (Table 1). Root prior assumptions did not have a significant effect on the model for ancestral state inference for the three transition rate model classes (e.g., equal rates + stationary root prior and equal rates + empirical root prior  $\Delta$ AICc<2). The equal rates model with an empirical root prior best fitted the data ( $\Delta$ AICc to next non-equivalent model = 23.41), inferring the intermediate flower type as the most likely ancestral state for clade II. In clade II, small flowers [staminate + carpellate] evolved on average 2.2 times with dioecy (95% confidence interval (CI) [1.7-2.8]), [staminate + intermediate] evolved on average 2.2 times with andromonoecy/cryptic dioecy (95% C.I. [2.1-2.4]), petaloid sepal flower types 2.2 times (95% CI [1.7-2.7]), and showy stamen flower types 1.4 times (95% CI [1-1.7]) (Fig. 2d). The ancestral state for clade I was inferred as most likely consisting of flowers with showy stamens, from which the petaloid sepal morphotype evolved once on average (95% CI [0.8-1.3]). The genus-level ancestral flower type could not be confidently resolved due to the inability to include outgroups using the flower morphotypes arising from our analyses within *Thalictrum*. Nevertheless, we were able to restrict the marginal probability (MP) for the ancestral flower type for the genus to two of the floral morphotypes: flowers with showy stamens (MP=51.6%) or the intermediate morphotype (MP=41.3%), with a much lower probability for flowers with petaloid sepals or unisexual flowers in the two dimorphic states (all three latter character states had MP<3%).

Refining pollination index boundaries in Thalictrum

We used pollination index (PI; Kaplan and Mulcahy 1971) as a summary indicator of pollination mode and as a separate method of assigning pollinator that can be scored from flower photos or herbarium specimens, enabling wider taxonomic sampling (83 species, compared to 29 in our morphology dataset). First, we calculated pollination index ranges for the five K clusters from PCA representing the three pollination modes, identifying the highest PI value for wind pollination and the lowest for insect pollination based on validated species. The more refined PI ranges were 1-1.29 for wind pollination and 2.57-3 for insect pollination, while intermediate values (1.3-2.56)

remained ambiguous (wind/ambophily/insect) (Table 1). *T. coreanum* had the lowest PI for an insect-pollinated group (2.43), but because it matched that of *T. lucidum* in the intermediate group, we conservatively set the next available value of 2.57 (*T. petaloideum*, excluding one outlier) as the lower bound for the insect pollination group. The intermediate cluster had a pollination index ranging from 1.43 (*T. guatemalense*) to 2.43 (*T. lucidum*).

To address whether multivariate analysis of pollination index would mirror the results from our continuous floral trait analyses, we conducted PCA of PI values. PC1 and PC2 accounted for 49.57% and 19% of the total variance, respectively [Supplementary data Fig. S6A], and K-means cluster analysis grouped species into "wind" (cluster 1), "wind/ambophilous" (cluster 2), and "insect" clusters (cluster 3) (K = 3) [Supplementary data Fig. S6B]. These results mostly coincide with the outcome of the pPCA, supporting the usefulness of PI in capturing the most informative morphological parameters in the absence of more comprehensive measurements from field-validated observations.

Reproductive organs show significant positive evolutionary correlation

To identify potential suites of co-evolving floral characters, we tested for evolutionary correlation while accounting for species variation, by fitting pairwise multivariate Brownian motion models in a Bayesian framework (Fig. 3). No significant negative correlations were found between floral traits, nor were most traits significantly evolutionary correlated (the posterior estimate of the correlation coefficient overlapped with zero for most traits tested; Fig. 3a-c, gray cells). However, 27 trait pairs exhibited strong positive evolutionary correlation (Fig. 3a-c, orange cells): 17 between reproductive traits (Fig. 3a), 5 between stamen and sepal traits (Fig. 3b), and 5 between carpel and sepal traits (Fig. 3c). Between reproductive traits, stamen and carpel lengths were positively correlated (Fig. 3a). The correlations between these two organs were likely driven by the positive correlation between their component parts: anther length with style length and anther length with stigma length (Fig. 3a). However, not all parts exhibited correlation. Importantly, filament length was

not positively correlated with any carpellate feature, and ovary length did not show positive correlation with staminate features, highlighting the modularity of stamens and carpels. Anther size, a composite trait between length and width, exhibited positive correlation with style length (Fig. 3c) that was likely driven in part by the positive correlation between anther length and style length.

There was also a positive evolutionary correlation between sepal number and size (width and length) in the carpellate and staminate datasets (Fig. 3b,c), and between stamen number and sepal size in the staminate dataset (Fig. 3c).

Traits with significant positive evolutionary correlation mirrored each other when mapped onto the phylogeny, as exemplified by anther size and style length (Fig. 3d and Fig. 3a highlighted cell). The observed evolutionary correlations are consistent with pollination syndromes in *Thalictrum*, where insect pollinated taxa tend to have smaller (shorter) anthers and short capitate stigmas, whereas wind-pollinated taxa tend to have larger (longer) anthers and longer styles and stigmas (Fig. 3d). Hence, clade I contains experimentally validated insect-pollinated species and exhibits cooler colors (i.e., shorter styles and smaller anthers), whereas clade II, where wind pollination has evolved repeatedly, contains a mix of dark and warmer colors (longer styles and smaller anthers). Subclade C provides further validation with its confirmed wind-pollinated taxa having longer reproductive structures (warmer branch colors).

#### **DISCUSSION**

We set out to detect different pollination syndromes in flowers of the ranunculid genus *Thalictrum* that lack synorganization (floral organ fusion), petals, and nectar, while exhibiting at least two distinct pollination modes (wind and insect). A substantially stronger reconstruction of relationships at the genus level, with increased taxon sampling and better resolved and supported subclades, was implemented to guide an unbiased exploration of floral morphospace via comparative analyses in the context of the evolution of wind pollination from insect-pollinated flowers. Flower morphology

can predict pollination mode in a subset of the species surveyed at the extremes of the distribution, possibly as a consequence of morphological convergence to pollination vectors combined with the evolutionary integration of floral traits. We propose that this evolutionary integration of traits likely compensates for the lack of floral synorganization, allowing for a certain degree of specialization to different pollination vectors. An intermediate floral morphotype identified via multivariate analysis was reconstructed as most likely ancestral for the clade where wind pollination evolved repeatedly, suggesting that this ancestral state may have provided an evolutionary testing ground that potentially led to adaptation to multiple pollination vectors.

Floral morphology as a proxy for pollination mode in Thalictrum

To test the degree to which floral morphology reflects the different pollination modes (wind, insect, or both) in *Thalictrum*, we employed clustering-based methods that employ predictions to fill gaps in natural history data and are therefore ideally suited for systems with a paucity of empirical data (van der Niet 2021). First, using both standard and phylogenetically informed multivariate analyses to visualize divergence across morphospace, we showed that continuous floral traits are able to partially discriminate between wind- and insect-pollinated taxa, with a less distinct morphospace that includes a mix of ambophilous, wind-, and insect-pollinated taxa. Then, we used these data to test the predictive power of a synthetic pollination index that summarizes seven key traits as a proxy for pollination mode.

Based on combined evidence from both these approaches, we set more precise ranges for using PI as an indicator of pollination mode when empirical data are not available and applied a clustering approach to increase predictability within the intermediate range. Partially overlapping boundaries in the intermediate PCA cluster are consistent with a more generalist, opportunistic pollination mode in *Thalictrum* (Robertson 1928; Kaplan and Mulcahy 1971; Melampy and Hayworth 1980; Motten 1986; Steven 2003). It thus appears that neither PI nor continuous floral traits can accurately discriminate between pollination modes within the species cluster with intermediate PI

values. Pollen release biomechanics is another, functional trait that discriminates wind- from insectpollinated species at the ends of the distribution but is less accurate at determining pollination mode
for those with intermediate PI values (e.g., *T. alpinum*, Timerman and Barrett 2019). Interestingly,
those species are newly classified as "ambiguous" in our adjusted PI boundary system (PI 1.43-2.43)
since they fall in our intermediate cluster, where predictions based on morphology are less accurate
and empirical studies are most needed. Whether based on quantification and evolutionary analyses
of flower morphology (this study) or on the biomechanical aspects of pollen release (Timerman and
Barrett 2019), there seems to be strong signal at the extremes of the wind-insect pollination
distribution, and a "gray" area of mixed features in the middle. We suggest that this intermediate
zone of floral morphospace, currently supported by two independent studies (Timerman and Barrett
2019 and this study), therefore not be discounted as a lack of power of floral morphometrics to
detect pollination syndromes, but rather be embraced as representative of a plastic space leading to
the use of either or both pollination vectors, depending on environmental circumstances.

Taken together, floral morphology is a better predictor of pollination mode for more specialized *Thalictrum* towards the extremes of the insect-wind adaptation spectrum. We hope that our study contributes to efforts towards improving pollination mode predictions based on floral morphology in *Thalictrum*. Other floral traits such as flower scent, mild overall in *Thalictrum* but richer in volatile compound diversity in the insect-pollinated species (Wang *et al.* 2019), and inflorescence architecture, known to be labile in other ranunculids (Zhao *et al.* 2012) may further contribute to better discrimination of pollination mode for species with intermediate flower morphologies. Complex functional traits, such as the ability of stamens to release pollen provide a promising venue (Timerman and Barrett 2021) but will be harder to dissect at the genetic level, given that they likely result from a variety of underlying developmental processes. The female side of wind pollination, pollen reception, is another key component that emerges as having evolutionary signal from our analyses in the form of style (and stigma) length, warranting further investigation.

Intermediate floral morphologies and ambophily as a step in the evolution of more specialized pollination modes

Here, we identified a floral morphotype in multivariate space, the intermediate cluster, that comprises all three pollination modes and hence appears more generalist than those in the other four PCA clusters. These less showy flowers are consistent with morphologies found in other ambophilous taxa (reviewed in Abrahamczyk et al. 2022). Two other morphotypes, consisting of petaloid sepals or showy stamens, appear to have converged on insect pollination via different morphological expressions of insect-attracting features, evolving in parallel at least twice in the genus (Fig. 2d). The last two morphotypes, consisting of small unisexual flowers (staminate and carpellate) with elongated sexual organs and small green sepals are strongly associated with wind pollination, which has evolved independently at least eight times (Wang et al. 2019). Phylogenetic reconstruction of these four more specialized flower morphotypes suggests that they more likely derive from an intermediate morphology within clade II. We have previously shown that insect pollination is ancestral not only for clade II but for the entire genus (Soza et al. 2012; Wang et al. 2019). Here, we propose that a generalist and potentially more plastic ancestral trait space, the intermediate cluster, enabled the subsequent evolution of a more specialized wind pollination mode, or a reversal to insect pollination in clade II of Thalictrum. Additional investigation of the pollination biology of species falling within the intermediate flower morphotype and the characterization of other discriminating traits are needed to further test the hypothesis that the intermediate morphotype represents an evolutionary transitional state. At the genus level, our analysis was able to limit the probable ancestral states to two floral morphotypes (showy stamens or intermediate morphologies), while excluding the other two (petaloid sepals or small unisexual flowers). An expansion of flower morphotype analyses to other Ranunculaceae is needed to further inform these hypotheses.

Evolutionary integration of floral traits: the role of selection and structural constraint

Floral integration tends to be higher in species with specialist pollinators compared to those with more generalist pollination modes (Pérez-Barrales et al. 2007; Rosas-Guerrero et al. 2011; Gómez et al. 2014). Floral integration is typically calculated from the variance in a trait correlation matrix for a given species (Wagner 1984; Cheverud et al. 1989). Fewer studies have explicitly modeled trait integration within a phylogenetic context (Joly et al. 2018; Kriebel et al. 2020), which requires fitting multivariate models of trait evolution in order to test for evolutionary correlation (Harmon 2018). As opposed to most other plants whose pollination biology has been placed in phylogenetic context (e.g., Smith et al. 2008; Lagomarsino et al. 2017; Reich et al. 2020), Thalictrum flowers lack organ fusion and whorled phyllotaxy (the latter often considered a morphological precursor of fusion, Endress 2016), both symplesiomorphic character states within angiosperms (Sauguet et al. 2017). While apetalous, nectar-less Thalictrum flowers are pollinated by a variety of generalist insects (Kaplan and Mulcahy 1971) and hence are not expected to exhibit specialized adaptations, morphological specialization to wind pollination has evolved repeatedly in the genus. In fact, our analyses identified traits that exhibit strong positive evolutionary correlation within the genus: between anther, style, and stigma lengths but not between stamen filament and ovary length, highlighting the modularity of stamens and carpels. The lengths of anthers, styles, and stigmas also appear to play an important role in segregating floral morphotypes in multivariate space based on the shared direction of their vectors in the biplots. The association between long, exserted stamens, styles and stigmas and wind pollination is often assumed (Friedman and Barrett 2009), yet it had not been tested explicitly within a phylogenetic framework. Given that we do not observe positive evolutionary correlation between all aspects of stamen and carpel morphology, e.g., filament length is not positively correlated with any carpel-related traits and ovary length is not positively correlated with staminate traits, we propose that these reproductive evolutionary correlations more likely result from the opposing selective pressures favoring abiotic versus biotic pollination than from structural constraints (such as allometry).

We also identified a positive evolutionary correlation between stamen number and sepal size in the staminate dataset, likely driven by sexual dimorphism in unisexual flowers, where staminate flowers tend to have bigger sepals than carpellate flowers. This sexual dimorphism has been previously postulated to result from an ectopic role of certain B-class genes, floral organ identity genes that specify petal and stamen identity, in sepals (Di Stilio *et al.* 2005; LaRue *et al.* 2013). In particular, certain *Thalictrum* homologs of the *APETALA3* lineage are differentially expressed in the perianth of staminate flowers, presumably making their sepals look larger and more petaloid than those of their carpellate counterparts (Galimba *et al.* 2018). Alternatively, this may be due to broader structural constraints, where flower meristem size is known to dictate the number and initial size of floral organ primordia (Moyroud and Glover 2017).

Our study offers novel insight into the common and difficult problem of assigning pollination mode when there are gaps in empirical data and into understanding whether and how suites of correlated floral characters evolve in concert in one of the few groups where wind pollination has evolved repeatedly within a genus. Even though a multivariate phylogenetic approach alone does not identify the ultimate causal processes underlying the observed correlations (Boucher *et al.* 2018), distinguishing convergent floral morphologies to specific pollination vectors from those due to shared descent brings us closer to that goal. Going forward, it would be desirable to achieve an evolutionary synthesis of all available sources of floral quantitative morphology and functional data to further identify tractable developmental and genetic indicators along the biotic-abiotic pollination spectrum.

Multiple paths towards wind pollinated morphologies are more likely than one

Given that wind pollination has evolved from insect pollination at least eight times in Thalictrum (Soza et al. 2012; Wang et al. 2019), we did not expect to find a single pathway from a flower morphology perspective. Evidence presented here supports the more likely scenario that *Thalictrum* species have used various paths emerging from an evolutionarily plastic, in flux floral morphospace associated with mixed pollination (whether stable or temporary) as a strategy to better exploit readily available wind for sexual reproduction under a putative shortage of insect pollinators. Thus, we find instances of multiple floral morphologies sharing the same pollination mode in what is best described as a morphotype continuum between insect and wind pollination.

#### SUPPLEMENTARY DATA

Supplementary data are available online at https://academic.oup.com/aob and consist of the following. **Table S1**: PCR and sequencing primers. **Table S2**: Phylogenetic models. **Table S3**: Voucher information. **Figure S1**: Representative flower scans and traits. **Figure S2**: Maximum likelihood *Thalictrum* phylogeny. **Figure S3**: Bayesian *Thalictrum* phylogeny. **Figure S4**: Variation in *Thalictrum* floral traits. **Figure S5**: Validation of Principal Component Analysis of *Thalictrum* floral traits. **Figure S6**: Principal Component Analysis of pollination index in *Thalictrum*. **Video S1**: First three dimensions of the PCA of *Thalictrum* floral traits.

#### **ACKNOWLEDGEMENTS**

We thank Simra Zahid for assistance with flower scans and measurements, University of Washington greenhouse staff for plant care, Dr. Sungwon Son for photographing *T. coreanum* flowers, and the Cornell University Statistical Consulting Unit for advice on statistical analysis. JMG thanks Elizabeth Mahood for the discussion on data dimensionality reduction and clustering methods. Two anonymous reviewers provided helpful comments that greatly improved the original manuscript.

#### **AVAILABILITY OF DATA AND MATERIALS**

Floral measurements, scripts, R package citations, alignments, and trees can be found in Zenodo (https://doi.org/10.5281/zenodo.6369383) upon publication.

#### **FUNDING**

This work was supported by National Science Foundation DEB [911539] and The Fred C. Gloeckner Foundation [630550] to VSD, Mary Sue Ittner Pacific Bulb Society grant to SRH, and National Science Foundation Graduate Research Fellowship [1650441] to JMG.

#### LITERATURE CITED

**Abrahamczyk S, Struck J-H, Weigend M**. **2022**. The best of two worlds: ecology and evolution of ambophilous plants. *Biological Reviews*.

Berg RL. 1960. The Ecological Significance of Correlation Pleiades. Evolution 14: 171–180.

Boucher FC, Démery V, Conti E, Harmon LJ, Uyeda J. 2018. A General Model for Estimating Macroevolutionary Landscapes. Systematic Biology 67: 304–319.

**Boyko JD**, **Beaulieu JM**. **2021**. Generalized hidden Markov models for phylogenetic comparative datasets. *Methods in Ecology and Evolution* **12**: 468–478.

**Charrad M, Ghazzali N, Boiteau V, Niknafs A**. **2014**. NbClust: An R Package for Determining the Relevant Number of Clusters in a Data Set. *Journal of Statistical Software* **61**: 1–36.

**Cheverud JM, Wagner GP, Dow MM**. **1989**. Methods for the Comparative Analysis of Variation Patterns. *Systematic Biology* **38**: 201–213.

**Culley TM, Weller SG, Sakai AK**. **2002**. The evolution of wind pollination in angiosperms. *Trends in Ecology & Evolution* **17**: 361–369.

**Darwin C**. **1862**. On the various contrivances by which British and foreign orchids are fertilized by insects, and on the good effects of interbreeding. London: John Murray.

**Davis SL**. **1997**. Stamens are not essential as an attractant for pollinators in females of cryptically dioecious Thalictrum pubescens Pursch. (Ranunculaceae). *Sexual Plant Reproduction* **10**: 293–299.

**Dellinger AS, Chartier M, Fernández-Fernández D, et al. 2019**. Beyond buzz-pollination – departures from an adaptive plateau lead to new pollination syndromes. *New Phytologist* **221**: 1136–1149.

**Delph LF, Galloway LF, Stanton ML**. **1996**. Sexual Dimorphism in Flower Size. *The American Naturalist* **148**: 299–320.

**Di Stilio VS, Kramer EM, Baum DA**. **2005**. Floral MADS box genes and homeotic gender dimorphism in Thalictrum dioicum (Ranunculaceae) – a new model for the study of dioecy. *The Plant Journal* **41**: 755–766.

**Drummond AJ, Ho SYW, Phillips MJ, Rambaut A. 2006**. Relaxed phylogenetics and dating with confidence. *Plos Biology* **4**: 699–710.

**Drummond AJ, Suchard MA, Xie D, Rambaut A**. **2012**. Bayesian phylogenetics with BEAUti and the BEAST 1.7. *Molecular Biology and Evolution* **29**: 1969–1973.

**Edgar RC**. **2004**. MUSCLE: multiple sequence alignment with high accuracy and high throughput. *Nucleic Acids Research* **32**: 1792–1797.

**Endress PK**. **2016**. Development and evolution of extreme synorganization in angiosperm flowers and diversity: a comparison of Apocynaceae and Orchidaceae. *Annals of Botany* **117**: 749–767.

**Fenster CB, Armbruster WS, Wilson P, Dudash MR, Thomson JD. 2004**. Pollination Syndromes and Floral Specialization. *Annual Review of Ecology, Evolution, and Systematics* **35**: 375–403.

Fenster CB, Reynolds RJ, Williams CW, Makowsky R, Dudash MR. 2015. Quantifying hummingbird preference for floral trait combinations: The role of selection on trait interactions in the evolution of pollination syndromes. *Evolution* 69: 1113–1127.

**Fior S, Li M, Oxelman B, et al. 2013**. Spatiotemporal reconstruction of the Aquilegia rapid radiation through next-generation sequencing of rapidly evolving cpDNA regions. *New Phytologist* **198**: 579–592.

**Friedman J, Barrett SCH**. **2009**. Wind of change: new insights on the ecology and evolution of pollination and mating in wind-pollinated plants. *Annals of Botany* **103**: 1515–1527.

**Galimba KD, Martínez-Gómez J, Di Stilio VS**. **2018**. Gene Duplication and Transference of Function in the paleoAP3 Lineage of Floral Organ Identity Genes. *Frontiers in Plant Science* **9**.

**Gómez JM, Perfectti F, Klingenberg CP**. **2014**. The role of pollinator diversity in the evolution of corolla-shape integration in a pollination-generalist plant clade. *Philosophical Transactions of the Royal Society B: Biological Sciences* **369**: 20130257.

**Guzmán D**. **2005**. Funciones masculina y femenina de la reproducción en cinco especies de Thalictrum (Ranunculaceae) con diferentes vectores de polinización. *Pirineos* **160**: 23–44.

**Hadfield JD**. **2010**. MCMC Methods for Multi-Response Generalized Linear Mixed Models: The MCMCglmm R Package. *Journal of Statistical Software* **33**: 1–22.

Harmon L. 2018. Phylogenetic comparative methods: learning from trees.

**Humphrey RP**. **2018**. Sterile stamens do not enhance seed set in females of the cryptically dioecious Thalictrum macrostylum (Ranunculaceae). *The Journal of the Torrey Botanical Society* **145**: 82–90.

**Hurvich CM, Tsai C-L**. **1989**. Regression and time series model selection in small samples. *Biometrika* **76**: 297–307.

Jolliffe IT. 2002. Principal Component Analysis. New York: Springer-Verlag.

Joly S, Lambert F, Alexandre H, Clavel J, Léveillé-Bourret É, Clark JL. 2018. Greater pollination generalization is not associated with reduced constraints on corolla shape in Antillean plants. *Evolution* 72: 244–260.

Kalyaanamoorthy S, Minh BQ, Wong TKF, von Haeseler A, Jermiin LS. 2017. ModelFinder: fast model selection for accurate phylogenetic estimates. *Nature Methods* 14: 587–589.

**Kaplan SM, Mulcahy DL**. **1971**. Mode of Pollination and Floral Sexuality in Thalictrum. *Evolution* **25**: 659–668.

**Kitazawa MS**. **2021**. Developmental stochasticity and variation in floral phyllotaxis. *Journal of Plant Research* **134**: 403–416.

**Kitazawa MS, Fujimoto K**. **2014**. A developmental basis for stochasticity in floral organ numbers. *Frontiers in Plant Science* **5**: 545.

Kriebel R, Drew B, González-Gallegos JG, et al. 2020. Pollinator shifts, contingent evolution, and evolutionary constraint drive floral disparity in Salvia (Lamiaceae): Evidence from morphometrics and phylogenetic comparative methods. *Evolution* 74: 1335–1355.

**Lagomarsino LP, Forrestel EJ, Muchhala N, Davis CC**. **2017**. Repeated evolution of vertebrate pollination syndromes in a recently diverged Andean plant clade. *Evolution* **71**: 1970–1985.

**LaRue N, Sullivan A, Di Stilio V**. **2013**. Functional recapitulation of transitions in sexual systems by homeosis during the evolution of dioecy in Thalictrum. *Frontiers in Plant Science* **4** 

**Melampy MN, Hayworth AM**. **1980**. Seed Production and Pollen Vectors in Several Nectar-Less Plants. *Evolution* **34**: 1144–1154.

**Motten AF**. **1986**. Pollination Ecology of the Spring Wildflower Community of a Temperate Deciduous Forest. *Ecological Monographs* **56**: 21–42.

**Moyroud E, Glover BJ**. **2017**. The Evolution of Diverse Floral Morphologies. *Current Biology* **27**: R941–R951.

**Nguyen L-T, Schmidt HA, von Haeseler A, Minh BQ**. **2015**. IQ-TREE: A Fast and Effective Stochastic Algorithm for Estimating Maximum-Likelihood Phylogenies. *Molecular Biology and Evolution* **32**: 268–274.

van der Niet T. 2021. Paucity of natural history data impedes phylogenetic analyses of pollinator-driven evolution. *New Phytologist* 229: 1201–1205.

**Ollerton J, Alarcón R, Waser NM, et al. 2009**. A global test of the pollination syndrome hypothesis. *Annals of Botany* **103**: 1471–1480.

Ollerton J, Rech AR, Waser NM, Price MV. 2015. Using the literature to test pollination syndromes---some methodological cautions. *Journal of Pollination Ecology* 16: 119–125.

**Parachnowitsch AL, Kessler A. 2010**. Pollinators exert natural selection on flower size and floral display in Penstemon digitalis. *New Phytologist* **188**: 393–402.

**Park Seongjun, Jansen RK, Park SeonJoo**. **2015**. Complete plastome sequence of Thalictrum coreanum (Ranunculaceae) and transfer of the rpl32 gene to the nucleus in the ancestor of the subfamily Thalictroideae. *BMC Plant Biology* **15**: 40.

**Pérez-Barrales R, Arroyo J, Armbruster WS**. **2007**. Differences in Pollinator Faunas May Generate Geographic Differences in Floral Morphology and Integration in Narcissus Papyraceus (Amaryllidaceae). *Oikos* **116**: 1904–1918.

**Phillips HR, Landis JB, Specht CD**. **2020**. Revisiting floral fusion: the evolution and molecular basis of a developmental innovation. *Journal of Experimental Botany* **71**: 3390–3404.

**Plummer M, Best N, Cowles K, Vines K**. **2006**. CODA: convergence diagnosis and output analysis for MCMC. *R News* **6**: 7–11.

**Posada D**. **2008**. jModelTest: Phylogenetic model averaging. *Molecular Biology and Evolution* **25**: 1253–1256.

**Powers JM, Seco R, Faiola CL, et al. 2020**. Floral Scent Composition and Fine-Scale Timing in Two Moth-Pollinated Hawaiian Schiedea (Caryophyllaceae). *Frontiers in Plant Science* **11**.

R Core Team. 2018. R: A language and environment for statistical computing.

Rambaut A, Drummond AJ, Xie D, Baele G, Suchard MA. 2018. Posterior Summarization in Bayesian Phylogenetics Using Tracer 1.7. Systematic Biology 67: 901–904.

**Reich D, Berger A, Balthazar M von, et al. 2020**. Modularity and evolution of flower shape: the role of function, development, and spandrels in Erica. *New Phytologist* **226**: 267–280.

**Revell LJ**. **2009**. Size-Correction and Principal Components for Interspecific Comparative Studies. *Evolution* **63**: 3258–3268.

**Revell LJ**. **2012**. phytools: an R package for phylogenetic comparative biology (and other things). *Methods in Ecology and Evolution* **3**: 217–223.

**Revell LJ, Harmon LJ**. **2008**. Testing quantitative genetic hypotheses about the evolutionary rate matrix for continuous characters. *Evolutionary Ecology Research* **10**: 311–331.

**Robertson C**. **1928**. *Flowers and insects; lists of visitors of four hundred and fifty-three flowers*. Carlinville, III.: n.p.

Ronquist F, Teslenko M, van der Mark P, et al. 2012. MrBayes 3.2: Efficient Bayesian Phylogenetic Inference and Model Choice Across a Large Model Space. Systematic Biology 61: 539–542.

Rosas-Guerrero V, Aguilar R, Martén-Rodríguez S, et al. 2014. A quantitative review of pollination syndromes: do floral traits predict effective pollinators? *Ecology Letters* 17: 388–400.

Rosas-Guerrero V, Quesada M, Armbruster WS, Pérez-Barrales R, Smith SD. 2011. Influence of Pollination Specialization and Breeding System on Floral Integration and Phenotypic Variation in Ipomoea. *Evolution* **65**: 350–364.

Sauquet H, von Balthazar M, Magallón S, et al. 2017. The ancestral flower of angiosperms and its early diversification. *Nature Communications* 8: 16047.

**Schneider CA, Rasband WS, Eliceiri KW**. **2012**. NIH Image to ImageJ: 25 years of image analysis. *Nature Methods* **9**: 671–675.

**Shaw J, Lickey EB, Schilling EE, Small RL**. **2007**. Comparison of whole chloroplast genome sequences to choose noncoding regions for phylogenetic studies in angiosperms: the tortoise and the hare III. *American Journal of Botany* **94**: 275–288.

**Smith SD**. **2016**. Pleiotropy and the evolution of floral integration. *New Phytologist* **209**: 80–85.

**Smith SD, Ané C, Baum DA**. **2008**. The Role of Pollinator Shifts in the Floral Diversification of lochroma (solanaceae). *Evolution* **62**: 793–806.

**Smith SD**, **Kriebel R**. **2018**. Convergent evolution of floral shape tied to pollinator shifts in lochrominae (Solanaceae)\*. *Evolution* **72**: 688–697.

**Soza VL, Brunet J, Liston A, Salles Smith P, Di Stilio VS. 2012**. Phylogenetic insights into the correlates of dioecy in meadow-rues (Thalictrum, Ranunculaceae). *Molecular Phylogenetics and Evolution* **63**: 180–192.

**Soza VL, Haworth KL, Di Stilio VS**. **2013**. Timing and consequences of recurrent polyploidy in meadow-rues (Thalictrum, Ranunculaceae). *Molecular Biology and Evolution* **30**: 1940–1954.

**Statisticat LLC**. **2021**. *LaplacesDemon: Complete Environment for Bayesian Inference*. Bayesian-Inference.com.

**Stebbins GL**. **1951**. Natural Selection and the Differentiation of Angiosperm Families. *Evolution* **5**: 299–324.

**Steven JC**. **2003**. Pollination and resource allocation in *Thalictrum* (Ranunculaceae): implications for the evolution of dioecy.

**Steven J, Waller DM**. **2004**. Reproductive alternatives to insect pollination in four species of Thalictrum (Ranunculaceae). *Plant Species Biology* **19**: 73–80.

**Tamura M**. **1995**. Ranunculaceae In: Hiepko P, ed. *Die Naturlichen Pflanzenfamilien*. Berlin, Germany: Duncker & Humblot, 223–497.

**Timerman D, Barrett SCH**. **2019**. Comparative analysis of pollen release biomechanics in Thalictrum: implications for evolutionary transitions between animal and wind pollination. *New Phytologist* **224**: 1121–1132.

**Timerman D, Barrett SCH. 2021**. The biomechanics of pollen release: new perspectives on the evolution of wind pollination in angiosperms. *Biological Reviews* **96**: 2146–2163.

**Tribble CM, Freyman WA, Landis MJ, et al. 2022**. RevGadgets: An R package for visualizing Bayesian phylogenetic analyses from RevBayes. *Methods in Ecology and Evolution* **13**: 314–323.

**Wagner GP**. **1984**. On the eigenvalue distribution of genetic and phenotypic dispersion matrices: Evidence for a nonrandom organization of quantitative character variation. *Journal of Mathematical Biology* **21**: 77–95.

Walker JD, Geissman JW, Bowring SA, Babcock LE, comps. 2018. *Geologic Time Scale v. 5.0.* Boulder, CO.

Wang TN, Clifford MR, Martínez-Gómez J, Johnson JC, Riffell JA, Di Stilio VS. 2019. Scent matters: differential contribution of scent to insect response in flowers with insect vs. wind pollination traits. *Annals of Botany* 123: 289–301.

**Whittall JB, Hodges SA**. **2007**. Pollinator shifts drive increasingly long nectar spurs in columbine flowers. *Nature* **447**: 706-U12.

**Wickham H. 2011**. ggplot2. *Wiley interdisciplinary reviews: computational Statistics* **3**: 180–185.

Wilke CO. 2020. cowplot: Streamlined Plot Theme and Plot Annotations for "ggplot2."

Yu G, Smith DK, Zhu H, Guan Y, Lam TT-Y. 2017. ggtree: an r package for visualization and annotation of phylogenetic trees with their covariates and other associated data. *Methods in Ecology and Evolution* 8: 28–36.

**Zhao L, Bachelier JB, Chang H, Tian X, Ren Y**. **2012**. Inflorescence and floral development in Ranunculus and three allied genera in Ranunculeae (Ranunculoideae, Ranunculaceae). *Plant Systematics and Evolution* **298**: 1057–1071.

**Table 1:** Flower morphotype and pollination mode assignment from multivariate analysis of floral traits in *Thalictrum* (Ranunculaceae). Field-validated pollination modes shown in bold (<sup>a</sup> Kaplan and Mulcahy 1971; <sup>b</sup> Melampy and Hayworth 1980; <sup>c</sup> Steven and Waller 2004; <sup>d</sup> Guzmán 2005). K means assignments (K=5 from PCA) provide new, more defined pollination index (PI) threshold values (thick lines): PI=1-1.29 for wind pollination and PI=2.57-3 for insect pollination. Intermediate values unresolved. PI estimates from Kaplan and Mulcahy 1971, Soza *et al.* 2012, Wang *et al.* 2019, and this study. \*Species with flowers split into more than one cluster were classified by the majority cluster (6/9 for *T. delavayi* and 5/6 for *T. petaloideum*). For dioecious and andromonoecious species, S = staminate, H = hermaphroditic, and C = carpellate.

Species	Flower Morphotype K=5	Pollination Mode From K-means	Pollination Index	
				T. thalictroides <sup>a</sup>
T. aquilegiifolium <sup>d</sup>	Showy Stamen	Insect	2.71	
T. delavayi*	Petaloid Sepal	Insect	2.71	
T. rochebrunianum	Petaloid Sepal	Insect	2.71	
T. clavatum <sup>b</sup>	Showy Stamen	Insect	2.57	
T. ichangense	Showy Stamen	Insect	2.57	
T. petaloideum*	Showy Stamen	Insect	2.57	
T. tuberiferum	Showy Stamen	Insect	2.57	
T. coreanum	Showy Stamen	Insect	2.43	
T. lucidum	Intermediate	Wind/Ambophily/ Insect	2.43	
T. flavum <sup>d</sup>	Intermediate	Wind/Ambophily/ Insect	2.29	
T. omeiense	Intermediate	Wind/Ambophily/ Insect	2.29	
T. uchiyamae	Showy Stamen	Insect	2.29	
T. kiusianum	Showy Stamen	Insect	2.14	
T. actaeifolium	Intermediate	Wind/Ambophily/ Insect	2	

T. alpinum <sup>c</sup>	Intermediate	Wind/Ambophily/ Insect	2
T. pubescens (S) <sup>a</sup>	Staminate	Wind	2
T. pubescens (H) <sup>a</sup>	Intermediate	Wind/ <b>Ambophily</b> / Insect	
T. elegans	Intermediate	Wind/Ambophily/ Insect	1.86
T. foetidum	Intermediate	Wind/Ambophily/ Insect	1.86
T. isopyroides	Intermediate	Wind/Ambophily/ Insect	1.86
T. minus <sup>d</sup>	Intermediate	Wind/Ambophily/ Insect	1.86
T. simplex	Intermediate	Wind/Ambophily/ Insect	1.71
T. guatemalense (S)	Staminate	Wind Wind/Ambophily/ Insect	1.43
T. guatemalense (H)	Intermediate		
T. revolutum (S) <sup>a</sup>	Staminate	Wind	1.29
T. revolutum (C) <sup>a</sup>	Carpellate		1.23
T. dasycarpum (S)	Staminate	Wind	1.14
T. dasycarpum (C)	Carpellate		
T. dioicum (S) <sup>c</sup>	Staminate	Wind	1.14
T. dioicum (C) <sup>c</sup>	Carpellate		
T. occidentale (S)	Staminate	Wind	1.14
T. occidentale (C)	Carpellate		
T. fendleri (S) <sup>c</sup>	Staminate	Wind	1
T. fendleri (C) <sup>c</sup>	Carpellate		
T. hernandezii (S)	Staminate	Wind	1
T. hernandezii (H)	Intermediate	Wind/Ambophily/ Insect	

## **Figure Captions:**

**Figure 1.** *Thalictrum* (Ranunculaceae) chronogram. Bayesian phylogeny and divergence time estimates for 99 *Thalictrum* taxa and 7 outgroups based on the analysis of six combined plastid regions in BEAST. Estimated mean ages (for main clades) and 95% highest posterior density (HPD) intervals shown at nodes. Two major clades, I and II, and three subclades with andromonoecious (A) and dioecious (B, C) members indicated. Taxa used for flower trait analyses are shown in red. Geologic epochs after (Walker *et al.* 2018).

Figure 2: Multivariate cluster analysis of floral traits. (a) Principal component analysis (PCA) of 17 floral traits across 29 species. Data points represent single flowers (N = 309) colored by K means cluster (top left) with symbols representing pollination mode (bottom right); representative flowers shown for each of five K-means clusters. PC1 discriminates flowers mostly by sexual system, segregating dioecious, wind-pollinated taxa (at both extremes of axis) from hermaphrodites comprising all 3 pollination modes at center of axis. PC3 further separates the central hermaphroditic flower cluster into three morphotypes, interpreted as petaloid sepals, showy stamens, and an intermediate morph, separating insect-pollinated species at its extremes from mixed pollinated taxa towards the center. H = hermaphroditic; PC = principal component (% of total variance explained). Colors represent K-means clusters (K = 5), with ad hoc assignment of flower morphology; filled symbols identify species with field-validated pollination mode data. (b) Biplot corresponding to PCA shown in (a), with loadings for the different floral traits represented as arrows towards larger values; the direction of the arrows indicates the contribution of each trait to the respective PC. (c) Top: Phylogenetic PCA (pPCA) of flower morphology in Thalictrum (Ranunculaceae). Dataset (from Fig. 2a) using species averages, with species names abbreviated to the first three letters. K-means analysis resulted in 3 clusters (K=3) enclosed in dashed lines, and available pollination mode information is shown with filled shapes as in (a), color-coding as in (d).

Bottom: PC combination from (a) that best matches the pPCA outcome (PC1 vs. PC2), for a direct comparison, showing a continuum of flower morphotypes and pollination modes along PC2. (d) Ancestral state reconstruction of flower morphotypes for 29 *Thalictrum* species from multivariate analysis shown in (a). The first three categories correspond to hermaphroditic sexual systems, while the last two encompass dioecy, andromonoecy, and cryptic dioecy (*T. pubescens*), respectively. Clades A-C as in Fig. 1. Pie charts represent the marginal probability (MP) of observing a certain flower morphotype (character state) at any given node.

Figure 3. Evolutionary correlation among floral traits in *Thalictrum* by multivariate Brownian motion. Correlation matrices for (a) reproductive floral organs (stamens and carpels), (b) carpellate dataset (from carpellate and hermaphroditic flowers), and (c) staminate dataset (from staminate and hermaphroditic flowers). The heat map shows the maximum *a posteriori* (MAP) estimates of the correlation coefficient for significant correlations; gray denotes no significant correlation, while orange indicates positive correlation (except in the diagonal, where it represents each trait against itself). No negative correlations were found. (d) Mirror trees exemplifying ancestral state reconstructions for two floral traits: anther size (left, with images to exemplify range) and style length (right, with images to exemplify range), highlighted in white in (a). Inferred MAP values (Inverse log +1) for ancestral nodes and tips are depicted with a color gradient on the phylogeny. Known pollination mode for species with field studies shown for reference: i = insect pollination, w = wind pollination, and w+i = ambophily (both). Scale bar within images = 1 mm.

**Appendix.** *Thalictrum* (Ranunculaceae) and outgroup samples used in this study for DNA extraction and phylogenetic analysis.

**Taxon**, *voucher* (Herbarium), GenBank accessions: *ndhA* intron, *ndhF*, *rbcL*, *rpl32-trnL* intergenic spacer, *trnL* intron and *trnL-trnF* intergenic spacer. Asterisks are voucher information for *trnL-trnF* region.

Aquilegia buergeriana var. oxysepala (Trautv. & C.A.Mey.) Kitam., Park AF01 (YNUH), JX258647, KM206671, JX258432, JX258540, JQ691534. A. formosa L., Di Stilio 128 (WTU), MT427936, MT427953, MT427984, MT427968, MT428001/MT428018. Enemion raddeanum Regal., Park ER01 (YNUH), JX258645, KM206669, JX258430, JX258538, JQ691533. Isopyrum manshuricum Kom., Park IM02 (YNUH), JX258646, KM206670, JX258431, JX258539, JQ691532. Leptopyrum fumarioides (L.) Reichb., Zhang s.n. (KUN), JX258650, KM206674, JX258435, JX258543, JX573531. Paraquilegia microphylla (Royle) J.R.Drumm. & Hutch., Liang s.n. (KUN), JX258649, KM206673, JX258434, JX258542, JX573530. Semiaquilegia adoxoides (DC.) Makino., Park SE01 (YNUH), JX258648, KM206672, JX258433, JX258541, JX573529. Thalictrum actaeifolium Siebold & Zucc., Yamazaki 1104 (TI), JX258544, KM206569, JX258329, JX258436, JX573432. *T. actaeifolium* var. *brevistylum* Nakai, Park 029 (YNUH), JX258545, KM206570, JX258330, JX258437, JX573433. T. acutifolium (Hand.-Mazz.) B.Boivin, Mu 180 (KUN), JX258637, KM206662, JX258423, JX258529, JX573521. T. alpinum L., Tatewaki 1074 (TI), JX258546, KM206571, JX258331, JX258438, JX573434. T. alpinum var. elatum O.E.Ulbr., Boufford 28521 et al. (TI), JX258549, KM206574, JX258334, JX258441, JX573437. T. amurense Maxim., unvouchered, MT427937, MT427954, MT427985, MT427969, MT428002/MT428019. *T. aquilegiifolium* L., *Kawahara 666 et al.* (TI), JX258550, KM206575, JX258335, JX258442, JX573438. T. aquilegiifolium var. sibiricum Regel & Tiling, Park 12 (YNUH),

JX258551, KM206576, JX258336, JX258443, JX573439. *T. arkansanum* B.Boivin, *Carr 17995* (TEX), JX258552, KM206577, JX258337, JX258444, JX573440. T. arsenii B.Boivin, Barriga 4750 (TEX), JX258554, KM206579, JX258339, JX258446, JX573442. T. atriplex Finet & Gagnep., Ho 2594 et al. (TI), JX258638, KM206663, JX258424, JX258530, JX573522. *T. baicalense* Turcz. ex Ledeb., *Quo 9156* (KUN)/Jeon s.n. (SKK)\*, JX258555, KM206580, JX258341, JX258448, JQ691506. T. calabricum Spreng., Segelberg s.n. (S), JX258556, KM206581, JX258342, JX258450, JX573443. T. calcicola T.Shimizu, Shimizu 10034 et al. (TI), JX258644, KM206668, JX258429, JX258537, JX573528. 7. chelidonii DC., Kanai 674743 et al. (TI), JX258639, KM206664, JX258425, JX258532, JX573523. T. clavatum DC., Kral 61853 (TEX), JX258557, KM206582, JX258343, JX258451, JX573444. T. confine Fernald, Fernald s.n. (TEX), JX258558, KM206583, JX258344, JX258452, JX573445. T. cooleyi H.E.Ahles, s.c. s.n. (OSC), MT427938, MT427955, MT427986, MT427970, MT428003/MT428020. T. coreanum H.Lév., Park 0501 (YNUH), JX258560, KM206585, JX258346, JX258454, JX573447. T. coriaceum (Britton) Small, Bozeman 10680 et al. (TEX), JX258561, KM206586, JX258347, JX258455, JX573448. *T. cuernavacanum* Rose, *Floden s.n.* (TENN), MT427939, MT427956, MT427987, MT427971, MT428004/MT428021. T. cultratum Wall., Qing 73-246 (KUN), JX258641, KM206665, JX258426, JX258534, JX573525. T. dasycarpum Fisch., C.A.Mey. & Avé-Lall., Carr 17991 (TEX), JX258563, KM206588, JX258349, JX258457, JX573450. *T. decipiens* B.Boivin, *Dillon 3126 et al.* (NY), JX258565, KM206590, JX258351, JX258459, JX573452. T. delavayi Franch., Boufford 27446 et al. (TI), JX258566, KM206591, JX258352, JX258460, JX573453. *T. diffusiflorum* C.Marquand & Airy Shaw, Liston 1161 (OSC), MT427940, MT427957, MT427988, MT427972, MT428005/MT428022. T. dioicum L., Wood 8903 and Wilson (TEX), JX258567, KM206592, JX258353, JX258461, JX573454. T. elegans Wall. ex Royle, Ludlow 20610 et al. (TI), JX258569, KM206594, JX258355, JX258463, JX573456. T. fargesii Franch. ex Finet & Gagnep., Boufford 26417 et al. (TI), JX258570, KM206595, JX258356, JX258464, JX573457. T. fendleri Engelm. ex A.Gray, Emily 5279 et al. (TEX), JX258571, KM206596, JX258357, JX258465, JX573458. T. filamentosum Maxim., Di Stilio 104 (WTU), MT427942, MT427959, MT427990, MT427973, MT428007/MT428024. T. finetii B.Boivin, Boufford 27614 et al.

(TI), JX258642, KM206666, JX258427, JX258535, JX573526. *T. flavum* L., *Soza 1908* (WTU), MT427947, MT427964, MT427995, MT427978, MT428012/MT428029. T. foeniculaceum Bunge, Smith 6618 (S), JX258573, KM206598, JX258359, JX258467, JX573460. T. foetidum L., Klackenberg 820619-6 (S), JX258574, KM206599, JX258360, JX258468, JX573461. T. foliolosum DC., Kanai 672444 and Shakya (TI), JX258575, KM206600, JX258361, JX258469, JX573462. *T. galeottii* Lecoy., Lucia 1125 (TEX), JX258576, KM206601, JX258362, JX258470, JX573463. T. gibbosum Lecoy., Pedro 8954 (TEX), JX258577, KM206602, JX258363, JX258471, JX573464. *T. grandiflorum* Maxim., *Tang 16* (PE), JX258578, KM206603, JX258364, JX258472, JX573465. *T. grandifolium* S.Watson, *Hinton 24708 et al.* (TEX), JX258579, KM206604, JX258365, JX258473, JX573466. *T. quatemalense* C.DC. & Rose, *Elias* 4989 (TEX), JX258580, KM206605, JX258366, JX258474, JX573467. T. heliophilum Wilken & DeMott, Waters s.n. (CS), MT427943, MT427960, MT427991, MT427974, MT428008/MT428025. T. henricksonii M.C.Johnst., Henrickson 13417 (RSA), MT427944, MT427961, MT427992, MT427975, MT428009/MT428026. T. hernandezii Tausch ex J. Presl, Pringle s.n. (S), JX258581, KM206606, JX258367, JX258475, JX573468. *T. ichangense* Lecoy. ex Oliv., *Park 31* (YNUH), JX258582, KM206607, JX258368, JX258476, JX573469. T. isopyroides C.A.Mey., Di Stilio 111 (WTU), MT427945, MT427962, MT427993, MT427976, MT428010/MT428027. T. kiusianum Nakai, Brunet s.n. (OSC), MT427946, MT427963, MT427994, MT427977, MT428011/MT428028. T. lankesteri Standl., Williams 11399 (NY), JX258583, KM206608, JX258369, JX258477, JX573470. T. lecoyeri Franch., Boufford 35394 et al. (PE), JX258643, KM206667, JX258428, JX258536, JX573527. *T. leuconotum* Franch., *Tang 0283 et* al. (PE), JX258584, KM206609, JX258370, JX258478, JX573471. *T. lucidum* L., Barabas 1131294 (PE), JX258585, KM206610, JX258371, JX258479, JX573472. T. macrocarpum Gren., Schultz s.n. and Winter (RSA), JX258586, KM206611, JX258372, JX258480, JX573473. T. macrostylum Shuttlew. ex Small & A.Heller, unvouchered, MT427948, MT427965, MT427996, MT427979, MT428013/MT428030. *T. minus* var. *hypoleucum* (Siebold & Zucc.) Miq., *Park 067* (YNUH)/*Park 051* (YNUH)\*, JX258587, KM206612, JX258373, JX258481, JQ691515. *T. myriophyllum* Ohwi, *Mori s.n.* (TI), JX258588, KM206613, JX258374, JX258482, JX573474. T. occidentale A.Gray, Karen 63 (TEX),

JX258589, KM206614, JX258375, JX258483, JX573475. *T. omeiense* W.T.Wang & S.H.Wang, *Wang* 519 (PE), JX258591, KM206616, JX258377, JX258485, JX573477. T. peltatum DC., Soule 2679 and Loockerman (TEX), JX258592, KM206617, JX258378, JX258486, JX573478. *T. petaloideum* L., Park 72 (YNUH), JX258593, KM206618, JX258379, JX258487, JX573479. *T. pinnatum* S.Watson, *Hemple 1067* and Jack (TEX), JX258594, KM206619, JX258380, JX258488, JX573480. *T. podocarpum* Kunth, Wiegend 2000/623 (OSC), MT427949, -, MT427997, MT427980, MT428014/MT428031. T. polycarpum (Torr.) S.Watson, Darin 0620 and Boyd (RSA), JX258596, KM206621, JX258382, JX258490, JX573482. *T. pringlei* S.Watson, *Walker s.n.* (NY), JX258598, KM206623, JX258384, JX258492, JX573484. T. przewalskii Maxim., Ho 2013 et al. (TI), JX258599, KM206624, JX258385, JX258493, JX573485. *T. pubescens* Pursh, *Moldenke 30097 and Moldenke* (TEX), JX258601, KM206625, JX258387, JX258495, JX573487. T. pubigerum Benth., Panero 4111 and Calzada (TEX), JX258603, KM206628, JX258389, JX258497, JX573489. T. punctatum H.Lév., Choi 60295 (YNUH), JX258604, KM206629, JX258390, JX258498, JQ691528. T. reniforme Wall., Naithani 37388 (TI), JX258605, KM206630, JX258391, JX258499, JX573490. T. reticulatum Franch., Boufford 42802 et al. (GH), MT427950, MT427966, MT427998, MT427981, MT428015/MT428032. T. revolutum DC., Fryxell 3756 (TEX), JX258606, KM206631, JX258392, JX258500, JX573491. T. rhynchocarpum Quart.-Dill. & A.Rich., Carvalho 3971 (NY), JX258608, KM206633, JX258394, JX258502, JX573493. T. rochebrunnianum Franch. et Sav., Park 106 (YNUH), JX258609, KM206634, JX258395, JX258503, JX573494. *T. rochebrunnianum* var. *grandisepalum* (H.Lév.) Nakai, *Uchima s.n.* (TI), JX258610, KM206635, JX258396, JX258504, JX573495. T. rostellatum Hook.f. & Thomson, Stainton 3392 and Williams (TI), JX258611, KM206636, JX258397, JX258505, JX573496. T. rotundifolium DC., Kanai 672698 and Shresta (TI), JX258612, KM206637, JX258398, JX258506, JX573497. T. rubescens Ohwi, Yamazaki 597 et al. (TI), JX258613, KM206638, JX258399, -, JX573498. T. rutifolium Hook.f. & Thomson, Boufford 29502 et al. (TI), JX258614, KM206639, JX258400, JX258507, JX573499. T. sachalinese Lecoy., Hara s.n. (TI), JX258615, KM206640, JX258401, JX258508, JX573500. T. saniculaeforme DC., Kanai 672443 and Shakya (TI), JX258616, KM206641, JX258402, JX258509,

JX573501. T. simplex var. brevipes H.Hara, Park 56 (YNUH), JX258617, KM206642, JX258403, JX258510, JX573502. *T. smithii* B.Boivin, *Boufford 28205 et al.* (TI), JX258618, KM206643, JX258404, JX258511, JX573503. *T. sparsiflorum* Turcz.ex Fisch.& C.A.Mey., *Jeon s.n.* (SKK), JX258620, KM206645, JX258406, JX258513, JQ691522. T. squamiferum Lecoy., Boufford 29603 et al. (TI), JX258621, KM206646, JX258407, JX258514, JX573505. T. squarrosum Stephan ex Willd., Smith 7560 (S), JX258622, KM206647, JX258408, JX258515, JX573506. T. strigillosum Hemsl., Hinton 139 et al. (TEX), JX258623, KM206648, JX258409, JX258516, JX573507. *T. tenue* Franch., *Smith 220* (S), JX258624, KM206649, JX258410, JX258517, JX573508. *T. texanum* (E.Hall ex A.Gray) Small, *Carr* 17939 (TEX), JX258625, KM206650, JX258411, JX258518, JX573509. T. thalictroides (L.) A.J.Eames & B.Boivin, Johm 37004 (TEX), JX258627, KM206652, JX258413, -, JX573511. T. trichopus Franch., Bartholomew 130 et al. (TI), JX258628, KM206653, JX258414, JX258520, JX573512. T. tripeltiferum B.Boivin, Detling 8788 (ORE), MT427951, N/A, MT427999, MT427982, MT428016/MT428033. T. tuberiferum Maxim., Park 055 (YNUH), JX258629, KM206654, JX258415, JX258521, JX573513. T. tuberosum L., Bremer 49 et al. (S), JX258630, KM206655, JX258416, JX258522, JX573514. T. uchiyamae Nakai, Park 156 (YNUH), JX258631, KM206656, JX258417, JX258523, JX573515. T. uncatum Maxim., Boufford 28389 et al. (TI), JX258632, KM206657, JX258418, JX258524, JX573516. T. uncinulatum Franch. ex Lecoy., Ho 1316 (PE), JX258633, KM206658, JX258419, JX258525, JX573517. T. urbainii Hayata, Liston 1162 (OSC), MT427941, MT427958, MT427989, -, MT428006/MT428023. *T. venulosum* Trel., *Shirakashi 52* (TEX), JX258634, KM206659, JX258420, JX258526, JX573518. *T. virgatum* Hook.f. & Thomson, *Boufford 30496 et al.* (TI), JX258636, KM206661, JX258422, JX258528, JX573520. *T. zernyi* Ulbr., *Gereau 3976 and Kayombo* (MO), MT427952, MT427967, MT428000, MT427983, MT428017/MT428034.

Figure 1

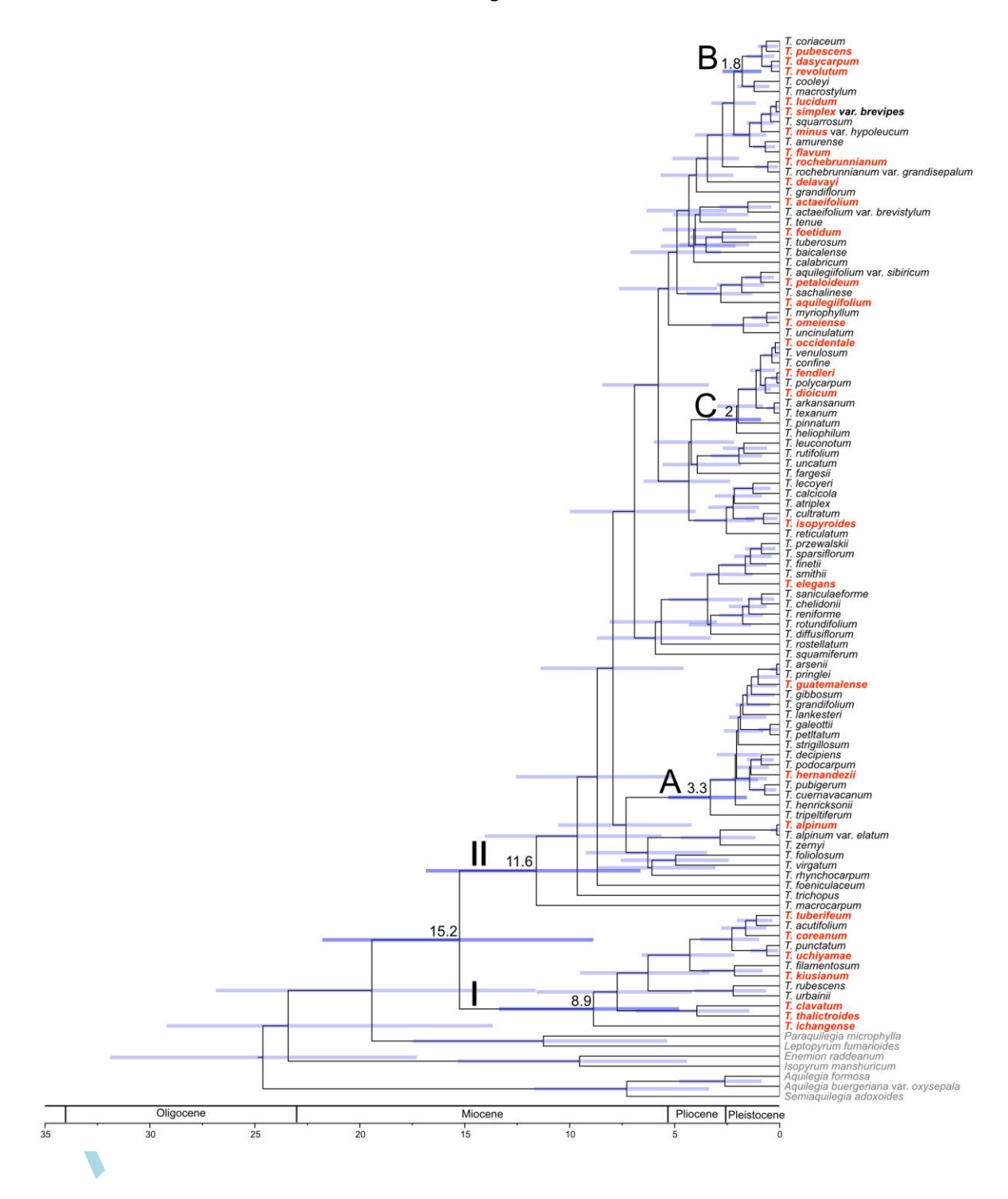


Figure 2

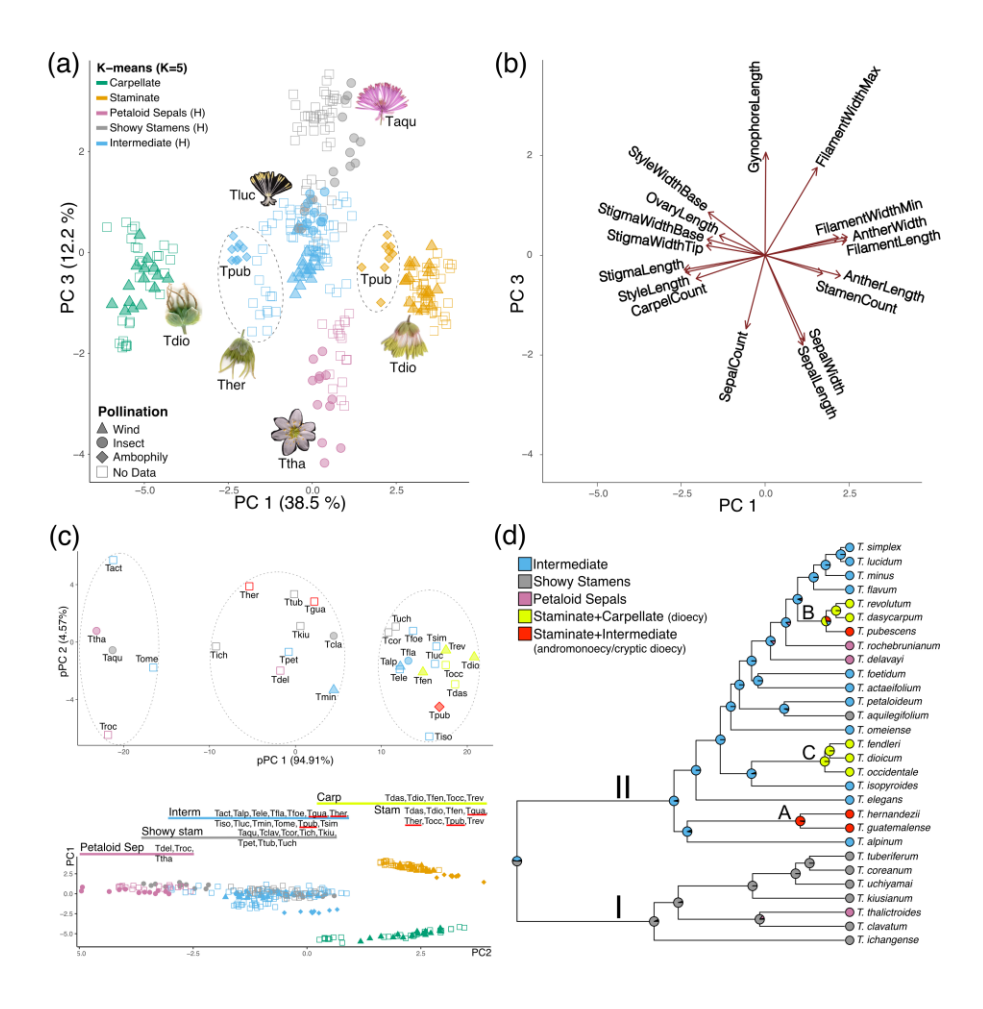


Figure 3

